Journal of Hip Preservation Surgery Vol. 3, No. 4, pp. 245–261
doi: 10.1093/jhps/hnw035
Review Article

REVIEW ARTICLE

Imaging of femoroacetabular impingement-current concepts

Christoph E. Albers[1,2,*], Nicholas Wambeek[3], Markus S. Hanke[2], Florian Schmaranzer[2], Gareth H. Prosser[1,4] and Piers J. Yates[1,4]

[1]Department of Orthopaedic Surgery, Fiona Stanley Hospital and Fremantle Hospital, Perth, Australia,
[2]Department of Orthopaedic Surgery, Inselspital, Bern University Hospital, University of Bern, Switzerland,
[3]Department of Radiology, Fiona Stanley Hospital and Fremantle Hospital, Perth, Australia and
[4]Faculty of Medicine, Dentistry and Health Sience, University of Western Australia, Perth, Australia
*Correspondence to: C. E. Albers. E-mail: christoph.albers@insel.ch
Submitted 16 April 2016; revised version accepted 12 September 2016

ABSTRACT

Following the recognition of femoroacetabular impingement (FAI) as a clinical entity, diagnostic tools have continuously evolved. While the diagnosis of FAI is primarily made based on the patients' history and clinical examination, imaging of FAI is indispensable. Routine diagnostic work-up consists of a set of plain radiographs, magnetic resonance imaging (MRI) and MR-arthrography. Recent advances in MRI technology include biochemically sensitive sequences bearing the potential to detect degenerative changes of the hip joint at an early stage prior to their appearance on conventional imaging modalities. Computed tomography may serve as an adjunct. Advantages of CT include superior bone to soft tissue contrast, making CT applicable for image-guiding software tools that allow evaluation of the underlying dynamic mechanisms causing FAI. This article provides a summary of current concepts of imaging in FAI and a review of the literature on recent advances, and their application to clinical practice.

INTRODUCTION

Since the description of femoroacetabular impingement (FAI), there has been increasing recognition and interest in this condition [1]. The understanding of the pathobiomechanics has evolved over the past decades leading to a variety of surgical treatment options including open [2] and arthroscopic procedures [3] with promising reported results [4–15]. Selecting the right patient for surgical treatment is imperative. Although the diagnosis is primarily made clinically, imaging plays a crucial role in the preoperative assessment. Over the past years, an increasing number of imaging modalities for the evaluation of FAI have made their way into clinical practice. While plain radiography and MR-arthrography (MRA) remain the gold standard in preoperative assessment [16], other imaging modalities including biochemical sequences of magnetic resonance imaging such as dGEMRIC as well as computed tomography (CT) and preoperative computer assisted animation and treatment simulation play an increasingly important role when evaluating pathologies associated with FAI [17–21].

The following article provides a literature review on preoperative evaluation of patients suffering FAI, highlighting the roles of different imaging modalities used in the detection of the underlying pathologies.

BACKGROUND FAI

FAI is a dynamic conflict of the hip defined by an early abutment of the proximal femur onto the acetabulum [1]. Intra-articular impingement is subdivided into cam- and pincer type FAI (Fig. 1). Cam Type FAI is predominantly the result of an aspherical contour at the antero-superior femoral head-neck junction that (when rotating into the acetabulum) applies compression and shearing forces at

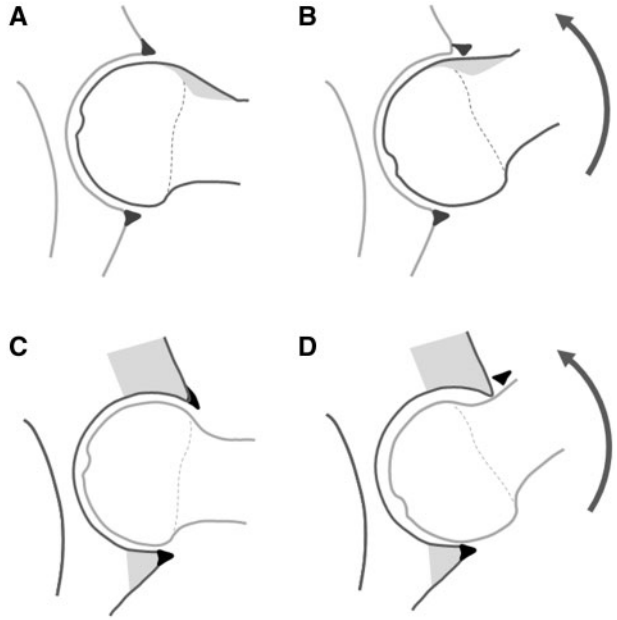

Fig. 1. The two pathomechanisms of intraarticular impingement are shown. (A) Cam-type impingement is caused by an asphericity of the femoral head-neck junction that when entering the acetabulum (B) applies shearing and compression forces to the articular cartilage. Frequently, fibrocartilaginous dissociation at the chondrolabral junction is observed. (C) Pincer-type impingement is caused by an overgrowth of the acetabular rim. (D) This leads to a compression of the labrum with labral tears. Often contre coup lesions are seen due to leverage of the femoral neck against the acetabular wall.

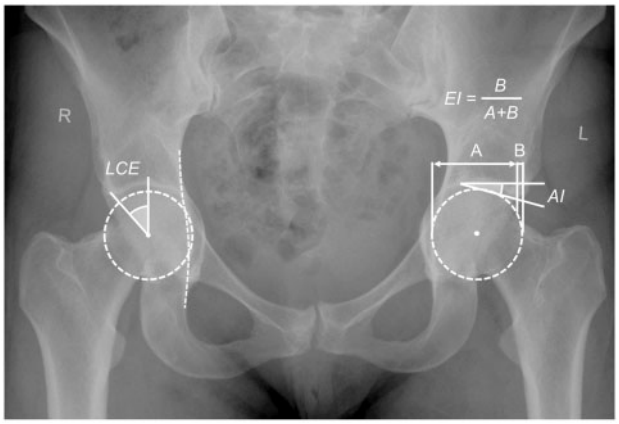

Fig. 2. The AP pelvic radiograph of a 26 years old female patient with bilateral general acetabular overgrowth and subsequent pincer type FAI is shown. The femoral head crosses the ilio-ischial line on both sides indicating acetabular protrusion. This is represented by an increased lateral center edge angle (LCE) >40°, a negative acetabular index (AI) and a decreased extrusion index (EI) <16%.

the chondro-labral junction leading to chondro-labral separation, degeneration of the labrum and detachment of the cartilage from the subchondral bone [1, 22]. Pincer type FAI is characterized by an excessive acetabular wall that results in a compression of the labrum between the femoral neck and the acetabular rim. Pincer type impingement is typically seen in hips with deep acetabula (i.e. acetabular protrusion, Fig. 2) or focal acetabular expansion (i.e. acetabular retroversion; [1, 22, 23]). Cam and pincer type FAI frequently occur concomitantly. While FAI describes the pathomechanism, the abnormal morphology can be caused by various underlying conditions such as Legg-Calvé-Perthes disease (LCPD) [24], slipped capital femoral epiphysis [25, 26] or post-traumatic deformities [27]. In the majority of cases, however, the etiology of FAI is developmental, or idiopathic.

PLAIN RADIOGRAPHY

Plain radiography is the primary imaging modality in the diagnostic process of FAI. It is cheap, fast, and widely available. Plain radiographs allow recognition of a wide variety of underlying hip disorders (i.e. Perthes disease, developmental dysplasia of the hip, slipped capital femoral epiphysis, etc.) and exclusion of preexisting advanced osteoarthritis (OA; [28]). In order to correctly interpret plain radiographs, standardized acquisition techniques have to be applied as plain films represent a 2D image of a 3D structure. Plain radiography is based on a point-shaped source with conical beam projection. Conical beam projection results in a more lateral projection of the object [29]. This is in contrast to CT utilizing a very narrow fan beam as small as 1 mm avoiding distortion of the object. Therefore, film-tube and patient-film distance, as well as centering and direction of the X-ray beam, and pelvic orientation during image acquisition have been proven to be factors with direct influence on the accuracy of the radiograph in the evaluation of hip morphology and pathology [30–34].

Film-tube distance affects the magnification of the object but also the projection of overlying 3D structures. In general, the closer an object to the X-ray source the larger its projection [29]. In the context of FAI, selected radiographic parameters can be influenced such as acetabular version: with increasing film-tube distance, acetabular anteversion increases and vice versa. Patient-film distance has been shown to be of minor importance as it remains relatively constant [30].

Centering of the X-ray beam plays an important role for the correct interpretation of radiographic parameters in FAI [30]. On the standard antero-posterior (AP) radiograph of the pelvis, the X-ray beam is centered between a line connecting both anterior superior iliac spines and the upper border of the symphysis. Acetabular orientation

varies considerably when the central beam is moved to another position, such as low-centered projections (routinely performed for hip arthroplasty) or hip-centered projection (Fig. 3). Both will result in an increase of the projected acetabular anteversion. A recent study compared differences of acetabular parameters obtained from AP pelvic radiographs and PA, hip centered fluoroscopy [35]. There were no differences between an AP pelvic radiograph and a PA hip centered fluoroscopic projection in terms of the lateral center edge angle (LCE; [41]), acetabular index (AI; [52]), ACM angle [42], Sharp's angle [43] and total femoral coverage [32]. However, compared with the AP pelvis radiograph, the anterior (posterior) femoral coverage was decreased (increased), the prevalence of a crossover sign was 30% lower, and the retroversion index underestimated on fluoroscopy [35].

Many radiographic parameters for the evaluation of FAI are highly dependent on the positioning of the patient during image acquisition [31, 33, 36]. Although AP pelvic radiographs are usually obtained according to a standardized protocol [16], variations of pelvic orientation are a natural consequence of a patient's posture, body habitus and level of discomfort with certain positions. Pelvic orientation can vary in three dimensions: pelvic tilt, pelvic rotation and pelvic obliquity. Malorientation can lead to misinterpretation of acetabular and pelvic parameters (Fig. 4). Inter-individual differences of up to 60° of pelvic tilt have been reported depending on patient's posture (standing versus supine; [37]). Variations of pelvic tilt can be assessed with the pelvic inclination angle on a true lateral pelvic radiograph. It is defined by the intersection of a line connecting the anterior border of the sacral promontory with the upper border of the symphysis and a horizontal line. Normal pelvic inclination has been found to be 60° [38–40]. Pelvic inclination can also be estimated by measuring the distance between the upper border of the symphysis and the midpoint of the sacro-coccygeal joint on the AP pelvic radiograph. The mean values for this vertical distance in a normal population have been reported to be 32 mm in men and 47 mm in women [36]. Pelvic malrotation is present if the center of the sacrococcygeal joint and the symphysis are not in line. Malrotation results in an increase of retroversion on the ipsilateral and an increase of acetabular anteversion on the contralateral side (Fig. 4; [31]). Alterations in pelvic obliquity can easily be overcome by assessing acetabular parameters with regard to a horizontal reference line such as the inter-tear drop line. A recent study [31] assessed the effect of pelvic tilt and rotation on 11 common radiographic hip parameters associated to FAI (LCE [41], AI [52], EI [16], ACM angle [42], Sharp angle [43], anterior and posterior acetabular coverage [32], crossover sign [44], retroversion index [36], posterior wall sign [44]). Using a validated computer software program (Hip^{2}Norm; [32, 45]), neutrally oriented radiographs were virtually rotated and tilted in pre-defined increments. Anterior and posterior acetabular coverage, cross-over sign, retroversion index and posterior wall sign changed significantly (Fig. 4) while LCE angle, acetabular-, extrusion index, ACM angle, Sharp angle and craniocaudal coverage remained unchanged [31].

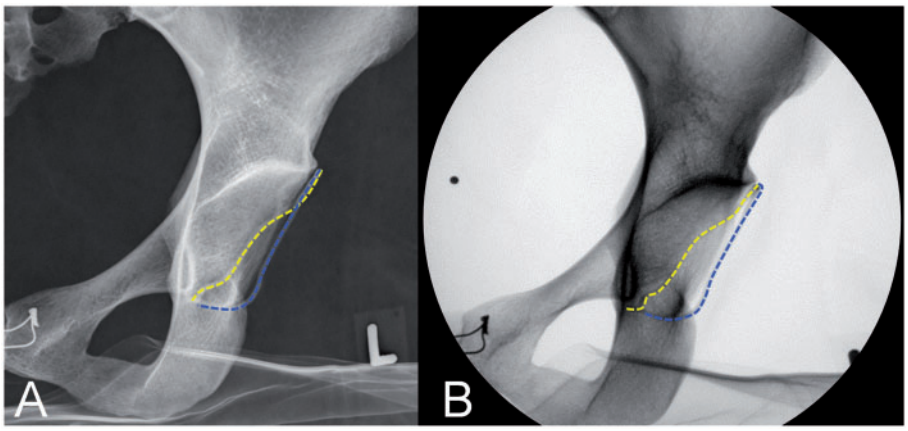

Fig. 3. The left hip of (A) an AP pelvic radiograph with the central beam directed to the center of the pelvis and (B) a PA hip centered fluoroscopic radiograph of the same cadaver pelvis is shown. The acetabular rim was marked with wires for better identification on the radiographs. Pelvic tilt and rotation was standardized for both projections. (A) On the AP radiograph, cranial retroversion with a positive crossover sign is present as the anterior wall (yellow dashed line) projects laterally to the posterior wall (blue dashed line) in the cranial portion of the acetabulum. On the hip centered fluoroscopy, the crossover sign is not depicted (anterior wall projects completely medial to posterior wall).

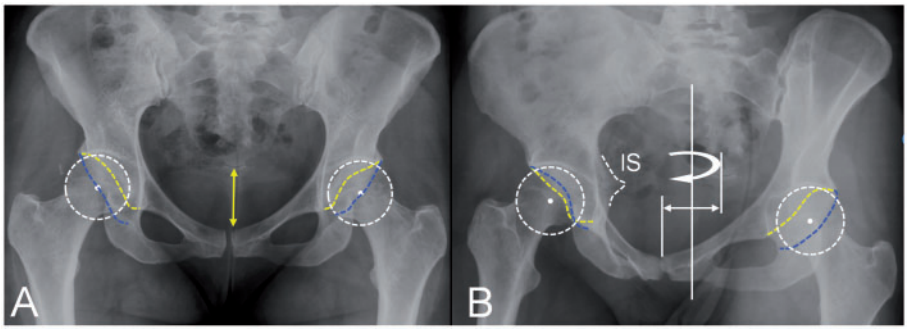

Fig. 4. Two AP pelvic radiographs of the same 33 year old female patient are shown. (A) The rotation of the pelvis during image acquisition is correct, the midline of the coccyx/sacrum and the symphysis are in line. The resulting projected, acetabular anteversion on both sides is normal: the anterior wall (yellow dashed line) projects medially to the posterior wall (blue dashed line). There is no positive posterior wall sign (= the center of the femoral head projects medially to the posterior wall). Pelvic tilt can be estimated by measuring the distance between the sacro-coccygeal joint and the upper boarder of the symphysis (yellow arrow). In females, a distance of 47 mm represents normal pelvic tilt [36]. (B) This pelvis was grossly malrotated to the right side during image acquisition which is represented by a malalignment between the midline of the coccyx/sacrum and the symphysis. On the right side, this results in false positive retroversion with nearly complete retroversion of the acetabulum represented by the anterior wall (yellow dashed line) projected laterally to the posterior wall (blue dashed line) on almost the entire length (retroversion index of 95%). The posterior wall sign and the ischial spine sign (IS) are positive. On the left side, because of the malrotation, the acetabulum appears excessively anteverted.

Radiographic projections in FAI

The routine radiographic projections for the evaluation of FAI pathomorphologies consist of an AP radiograph of the pelvis as well as a lateral view of the proximal femur [16, 46]. Additional projections include the Dunn Rippstein Müller view and modified Dunn view [47, 48], frog leg view and Lauenstein view [49], false profile view [50] or true lateral view of the pelvis. Radiographs performed for FAI allow assessment of both femoral and acetabular/pelvic pathomorphologies, including depth, coverage and orientation on the acetabular side, as well as head sphericity, head-neck offset and torsion on the femoral side. Additional findings may include joint incongruency due to several underlying hip pathologies.

Acetabular depth is assessed on the AP pelvic radiograph. It is quantified by the coxa profunda and protusio acetabuli sign. Coxa profunda is defined as positive if the acetabular socket touches or crosses the ilio-ischial line. Acetabular protrusion is present, if the femoral head touches or crosses the ilio-ischial line (Fig. 2). Nepple *et al.* found no differences in the prevalence of the coxa profunda sign between normal hips and pincer impingement. It was therefore concluded that the profunda sign may be considered a normal radiographic finding [51]. On plain radiographs, lateral acetabular coverage is assessed by the LCE angle [41], the AI [52] and the EI [53]. The LCE angle is defined by a line connecting the center of the femoral head and the lateral edge of the acetabular sourcil and a vertical reference line (Fig. 2; [41]). While a low LCE angle is pathognomonic for developmental dysplasia of the hip [53], abnormally high LCE angles account for pincer type FAI (Fig. 2). There is controversy regarding both the lower and upper threshold values. Most studies refer to lower cut off values, however, values of 34–39° have been found in patients suffering pincer type FAI requiring isolated acetabular rim trimming, while an angle of above 40° was found in hips with protrusio acetabuli [54]. Tönnis *et al.* defined values between 39° and 44° in hips with a deep acetabulum and values above 44° in hips with acetabular protrusion [52]. The AI is defined by a line connecting the medial and lateral edge of the acetabular sourcil and a horizontal reference line (Fig. 2; [52]). High AI is found in dysplastic hips, while low AI is associated with overcoverage. The normal range of the AI has recently been defined between 3° and 13° [54]. Angles below 3° were found in hips with pincer type FAI and hips with acetabular protrusion [54]. The extrusion index is measured on the AP pelvic radiograph and is defined as the percentage of femoral head that is not covered by the acetabulum (Fig. 2; [53]). The cut off from normal to over-coverage has previously been defined at >16% [54]. Values between 0 and 16% were reported to be associated pincer FAI induced OA [55]. The anterior femoral head coverage is assessed by the anterior center edge (ACE) angle on the false profile view described by Lequesne and Sèze [50]. The ACE angle is constructed by a line connecting the center of the femoral head and the anterior edge of the acetabular sourcil and a second vertical reference line.

While values below 25° are associated with dysplastic hips, angles above 41° was found in hips with pincer type FAI [56]. Posterior coverage is assessed qualitatively by the posterior wall sign on the AP pelvic radiograph [44]. The posterior wall is deficient, if the contour of the posterior acetabular rim lies medially to the femoral head. This is frequently found in acetabular retroversion that is associated with anterior overcoverage. The acetabular wall index semiquantitatively assesses anterior and posterior femoral head coverage on the AP pelvic radiograph. It is defined as the ratio of the distance of anterior (posterior) wall covering the femoral head and the radius of the femoral head [57].

In a normally anteverted hip, the contour of the anterior wall is projected completely medially to the contour of the posterior wall. Retroversion is visualized by partial or complete lateral projection of the anterior wall in relation to the posterior wall, which was first described by Reynolds *et al* as the 'cross over sign' (Fig. 4; [44]). The posterior wall sign is positive if the posterior wall is located medially to the femoral head center (Fig. 4; [44]). However, it can be present with posterior wall deficiency without concomitant anterior wall overgrowth. The retroversion index is a quantitative measure using the ratio of the retroverted craniolateral acetabular opening to the entire opening of the acetabular socket [16]. Another parameter indicative of retroversion, the 'ischial spine sign', is present if the ischial spine projects medially to the ilio-pubic line (Fig. 3; [58]). Tannast *et al* showed in their study that retroversion was not an isolated pathomorphology of the acetabulum but of the entire hemipelvis externally rotated [59]. It was recently shown that the size of the lunate surface in retroverted acetabula did not differ compared to normal hips [60].

Several radiographic parameters exist to analyse the cam lesion, most of which appear on the axial 'cross-table'-, Dunn- or Lauenstein view due to the typical location of the asphericity at the antero-superior femoral head-neck junction. The alpha angle is comprised by a line connecting the femoral head center and the point where the anterior head-neck contour exceeds the femoral head radius (Figs. 5 and 7). An angle above 50° has been found to be associated with cam-type FAI [61]. Although the alpha angle has only been validated on the cross-table view [61], the alpha-angle is commonly measured on almost all other projections of the proximal femur. The complementary angle at the posterior head-neck junction is called beta angle [62]. Femoral head-neck offset is another measure to characterize a cam deformity [61, 63]. The head-neck offset is typically reduced in cam type FAI [61, 63]. The femoral head-neck offset is defined as the distance between a line parallel to the femoral neck axis passing tangentially through the widest diameter of the femoral head and a parallel line that passes through the point where the femoral head-neck contour exceeds the femoral head radius [16, 63]. The femoral head-neck offset is reduced in aspherical heads with low neck-width to head-radius ratio (Fig. 11). It has been shown to become negative in cases of slipped capital

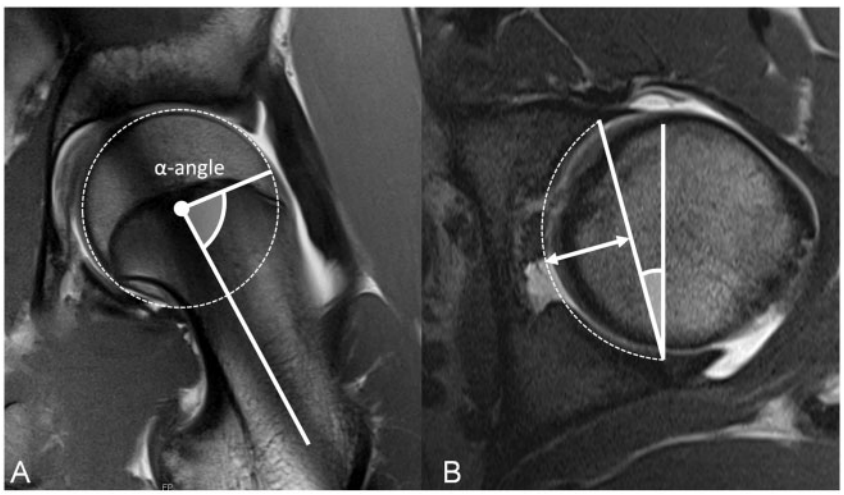

Fig. 5. (A) A radial proton density weighted MRA slice (1 o'clock position) of a 21-year-old male patient with an increased alpha angle of 85° is shown. The alpha angle is comprised by the femoral neck axis and a line connecting the femoral head neck center and the point where the anterior head-neck contour exceeds the femoral head radius. (B) Acetabular version can be measured on axial MRI/MRA sequences. Version is comprised by a line connecting the posterior and anterior margins of the acetabular rim at labral attachment site onto the acetabular wall and the sagittal axis. Note that acetabular version cannot be corrected for pelvic tilt and rotation on MRI/MRA of the hip. Acetabular depth (arrow) is measured as the distance between the line connecting the acetabular margins and a parallel line tangential to the deepest point of the acetabular socket [82].

femoral epiphysis [25]. On the AP pelvic radiograph, the asphericity of the femoral head-neck junction can appear as a pistol grip deformity [64]. Severe asphericities such as sequelae of LCPD appear with a sagging rope sign on the AP radiograph [65].

Additional findings related to FAI include torsional deformities of the femur as well as coxa vara and coxa valga [66]. Coxa vara and valga are quantified using the center-collum-diaphyseal (CCD) angle on AP pelvic radiographs. In normal hips, the CCD angle ranges between 129° and 135° [62, 67]. It appears too high with external rotation. The assessment of femoral torsion is best achieved by 3D imaging modalities. However, plain radiography allows the assessment of femoral torsion according to the techniques described by Dunn, Müller and Rippstein [47, 48, 68]. Finally, although cut off values for the majority of radiographic parameters associated with FAI have been defined, it is important to note that a variety of studies reported pathologic radiographic findings both on the acetabular and femoral side in completely asymptomatic patients [69–74]. Thus, the diagnosis of FAI syndrome and subsequent treatment indications must never be based on the presence of plain radiographic parameters alone but must be correlated with clinical findings and further imaging.

MAGNETIC RESONANCE IMAGING

MRI and MRA of the hip are essential imaging modalities in the preoperative work up of FAI [16, 75–81]. Examinations are optimally performed on a 3T MRI unit for maximal spatial resolution. Dedicated small field of view imaging is used for optimal labral and cartilage evaluation. MRI with MRA provides information on articular cartilage and labral injury as well as osseous pathology and any surrounding soft tissue abnormality around the hip. Sequences are performed post intra-articular injection of gadolinium (MRA), and typically include three plane Fat saturated T1 sequences (Coronal, Sagittal and Axial oblique in the plane of the femoral neck), Fat saturated fats Spin Echo (FSE) T2 in the coronal and Sagittal plane, and axial T1 or PD sequences and Radial FSE PD or volumetric thin slice GRE allowing radial reconstructions along the axis of the femoral neck (or any other plane). As an alternative to reconstructing radial slices from 3D volumetric data, higher resolution and subsequent more accurate assessment is achieved from separate radial proton density weighted sequences that are based on a sagittal oblique localizer from coronal sequences [77]. A Coronal T1 weighted sequence without Fat saturation may also be useful for osseous evaluation. Technical difficulties of MRI/MRA in the evaluation of FAI related pathomorphologies are encountered with the deep location of the hip within the body with thin cartilage layers, a spherical shape of the joint requiring both a high signal-to-noise ratio as well as high spatial resolution [78]. Although technical progress has been made including high MR strength field, cartilage specific sequences and movable surface coils, it remains challenging to obtain a conclusive evaluation of the general status of the articular cartilage in the hip joint. To date, there is no comprehensive classification system stratifying the degree of osteoarthritis of the hip based on MRI/MRA.

MRI/MRA is very useful to assess morphologic parameters related to the osseous configuration of both the acetabulum and the proximal femur. These include depth (Fig. 5) and width [82], femoral head coverage [60, 82] or version (Fig. 5; [82]) on the acetabular side and the alpha angle (Fig. 5) as well as femoral head neck offset [25, 61], and tilt and epiphyseal angles [25] on the femoral side. Multiplanar reconstructions render the potential of a 3D assessment of the hip joint allowing depiction of the exact location and extent of the pathomorphology associated with FAI. Radial sequences around the axis of the femoral neck providing the possibility to assess the 3D geography

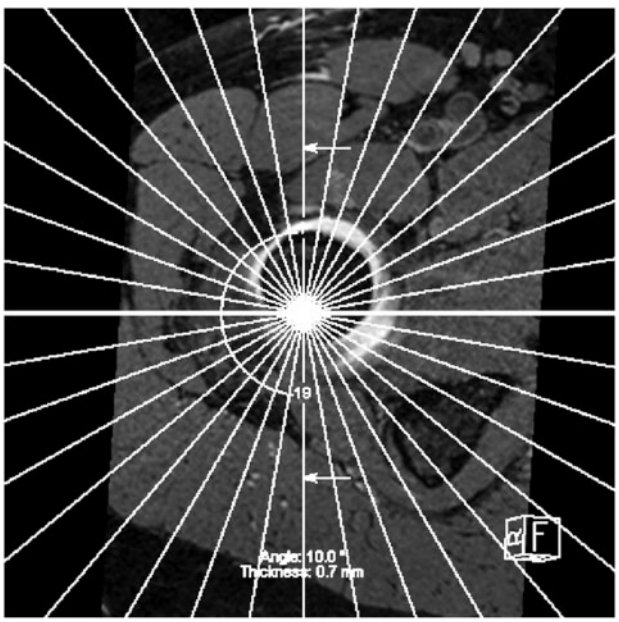

Fig. 6. The arrangement of radial MR-sequences rotating around the femoral neck axis are shown. This allows a three dimensional assessment of the hip joint in a clockwise fashion depicting FAI associated lesions that are frequently prevalent in the antero-superior quadrant (3 o'clock to 12 o'clock) and corresponding postero-inferior quadrant (6 o'clock to 9 o'clock). Radial slices can be reconstructed from 3D volumetric datasets. Higher resolution is achieved by obtaining separate radial proton density weighted sequences based on a sagittal oblique localizer.

of the acetabulum have proven to be very useful both in diagnosis and planning (Fig. 6; [16, 77, 83]). A study by Dudda *et al.* compared the alpha angles on plain AP and cross-table radiographs with radial MRA slices of the femoral head neck junction (Fig. 5; [83]). The authors found increased alpha angles at the antero-superior head neck junction on MRA in hips that had a normal appearance on plain radiographs [83]. Another recent study confirmed these findings and noted the highest correlation between increased alpha angles measured on radial MRI sequences and plain films on the 45° Dunn view representing the anterosuperior portion of the head neck junction [84]. A recent MRA based study investigated the three dimensional femoral head coverage as well as the shape of the lunate surface using the outer and inner center edge angles [60]. The authors demonstrated significant differences of both size and shape of the lunate surface between hips with acetabular retroversion, deep acetabula, acetabular protrusion and normal/asymptomatic hips thereby providing theoretical implications for joint preserving surgical treatment of each entity [60]. Acetabular version can be assessed in the axial plane using MRI/MRA (Fig. 5). Previous studies reported distinct differences of acetabular version depending on the cranio-caudal level at which the measurements were performed: whereas decreased version was found at the more cranial sections below the acetabular dome, more pronounced anteversion was present when the measurements were performed at the level of the femoral head center [82, 85–87].

Next to the assessment of bony lesions, MRI/MRA allow an excellent assessment of intra- and extraarticular soft tissue structures, particularly labral and chondral abnormalities [88, 89]. Labral lesions include alterations in size (hypo-/hyperplastic), labral tears and intrasubstance changes. Labral tears can appear as chondro-labral separation, partial and complete labral undersurface tears, intrasubstance tears or complex labral tears (Fig. 7). Intrasubstance changes include mucoid degeneration, calcific changes, ossification of the labrum, or labral ganglia [22, 90–92]. There is no sophisticated classification system on MRI relating to FAI associated labral lesions. Czerny *et al.* [93] introduced their classification in 1996 prior to the introduction of the femoroacetabular impingement concept. Cartilage lesions can be partial and full thickness lesions. Full thickness lesions are subdivided in defects or delamination from the subchondral bone. Delamination occurs as bubbles (chondral detachment from bone with intact periphery), pockets (cartilage detached from bone with one open edge) or flaps (cartilage detached with more than one open edge; [22, 90–92]). The overall sensitivity (specificity) by two readers to detect cartilage delamination by a subchondral contrast agent collection on MRA has been found in 22 and 30% (95 and 95%) of the cases compared with the intraoperative analysis [80]. In pincer type FAI, typical findings include partial ossification of the labrum with possible labrum avulsion. Fibrocystic lesions at the femoral head-neck junction (herniation pit or linear indentation sign) are occasionally seen [16]. Cartilage lesions involve large areas of thin cartilage that may be associated with a posteroinferior contre-coup cartilage lesion ([81]; Fig. 1D). Cam impingement

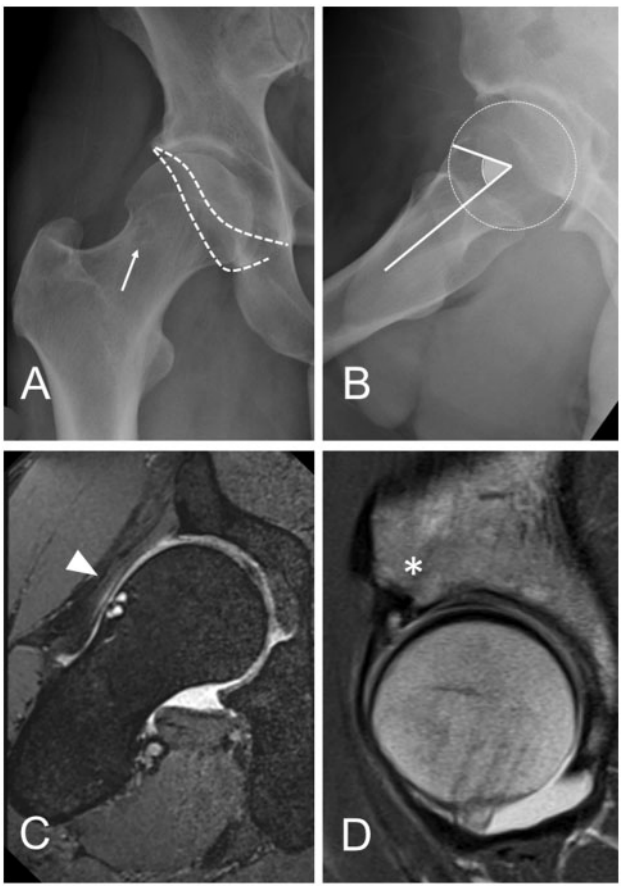

Fig. 7. Preoperative images of a 33 years old male with cam type FAI are illustrated. (A) The AP pelvic radiograph reveals an asphericity at the femoral head-neck junction with a radiolucent herniation pit (arrow). The acetabulum shows normal version with a negative cross over sign (white dashed lines). There are no posterior wall deficiencies (negative posterior wall sign). (B) On the frog leg view, the alpha angle is increased. (C) Radial MRI images (TRUFI sequences) confirm the high signal intensity herniation pit at the 1 o'clock position (arrow). In addition, the asphericity of the femoral head neck junction is depicted. (D) Sagittal slices of proton density weighted MRI sequences are shown. An undersurface labral tear is depicted anterosuperiorly as a result of the aspherical femoral head entering the acetabulum (asterisk).

involves cartilage lesions that are larger in width and more focal. Often, cartilage delamination from the subchondral acetabular bone is present with associated undersurface tears of the labrum [80, 88].

The intraarticular injection of contrast agent facilitates the diagnosis of chondral and labral lesions by separating intraarticular structures and delineating the anatomy [88]. A recent prospective study proved superiority of MRA versus non-contrast MRI with regard to the detection of labral tears and partial thickness acetabular cartilage lesions compared with the intraoperative findings [94]. The sensitivity to depict labral tears was 81 and 69% with MRA and 50 and 50% on MRI for two different readers. Acetabular cartilage defects had a sensitivity of 71 and 92% on MRA and 58 and 83% on MRI. There were no differences with regard to the detection of cartilaginous lesions of the femoral head [94]. A recent meta-analysis revealed a sensitivity and specificity of 83 and 57% respectively using MRA for labral lesions [95]. Other studies reported similar sensitivities (specificities) ranging between 85 and 97% (33–100%) on MRA [93, 94, 96]. A recent study comparing preoperative MRI and MRA with the arthroscopic findings in 43 hips reported a near equivalent sensitivity for the detection of labral lesions using MRA (sensitivity, 90–93%) and MRI (sensitivity, 88–90%). However, superior results were noted for the detection of acetabular cartilage lesions using MRA (sensitivity, 71–81%) compared with MRI (sensitivity, 58–65%; [97]).

Traction MRA

Cartilage delamination from the subchondral bone is a frequent finding in hips with cam-type FAI. However, femoro-acetabular coaptation prevents contrast agent from undermining this subchondral space resulting in a misjudgment/underestimation of the lesion [88, 98–100]. To achieve better radiographic visualization of the chondrolabral interface and the articular cartilage layers, the application of axial leg traction during MRA has previously been proposed [90, 101–103]. Prior to the application of traction with the hip slightly flexed, 10–27 ml of iodinated contrast agent (1–2 ml), local anesthetic (2–5 ml) and diluted MR contrast agent (10–20 ml) are injected into the joint under fluoroscopic guidance [90, 101, 102]. MR-compatible traction devices are routinely used for continuous traction during the examination. Traction devices consist of a pulley system, a cable or rope connected to the leg either with an ankle brace [90, 102] or with adhesive straps for skin traction [101]. A weight is connected to the other end. The contralateral leg can be stabilized to avoid tilting of the pelvis to the side where axial traction is applied [90, 102]. The amount of traction varies between 6 and 23 kg for a period ranging between 3 and 19 min among different studies [90, 101–103]. Temporary traction is tolerated well without complications [90, 101, 102]. MRA with traction results in separation of the femoral and acetabular articulating surfaces [101]. This allows

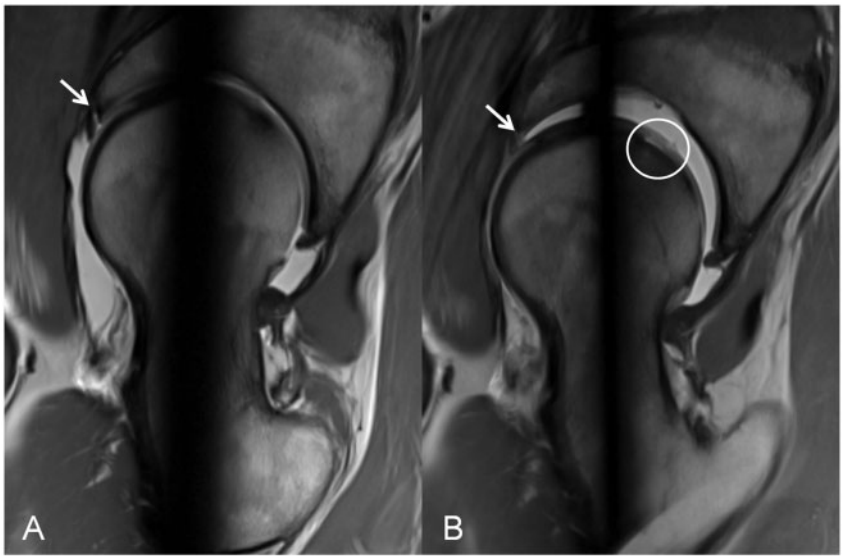

Fig. 8. A 25-year-old-woman with surgically confirmed cartilage delamination at the femoral head due to traumatic hip subluxation is shown. Direct MR arthrograms (2D radial PD-weighted images) without (A) and with leg traction (B). (A) A partial labrum tear can be seen (arrow). Without traction the cartilage seems intact. (B) Traction (18 kg) leads to joint distraction and concomitant accumulation of contrast agent between cartilage layers. Subchondral contrast accumulation and disrupted femoral cartilage surface corresponding to chondral delamination becomes visible (circle).

delineation of the femoral and acetabular cartilage layers (Fig. 8). However, in a recent study complete separation between the cartilage layers was achieved in only 8% after applying 8-10kg of traction and 10-14ml injection of contrast agent [103]. A recent study utilizing MRA with traction reported the detection of acetabular cartilage lesions with a sensitivity of 85–88% and specificity of 78–96% for two different readers [90]. In most cases, contrast agent accumulated in the pathologic, subchondral space. The same study reported the depiction of femoral cartilage lesions with a sensitivity of 81–86% and a specificity of 91–94% respectively [90]. This is in contrast to studies obtaining images from MRA without traction reporting a sensitivity (specificity) ranging between 40 and 83% (41–91%) [94, 104, 105].

Biochemical MRI/MRA

Evidence suggests that successful outcome after surgical intervention in patients with FAI depends on the degree of pre-existing joint degeneration [4, 106]. It is therefore critical to identify patients with FAI in an early phase of chondrolabral damage prior to the onset of irreversible degeneration to achieve a successful outcome after joint preserving surgery. Recent developments include biochemically sensitive MRI sequences. Biochemical MRI has been shown to reproducibly detect and quantify alterations of the extracellular cartilage matrix. These alterations include the reduction of extracellular glycosaminoglycan, cartilage matrix (de)hydration and collagen fiber integrity. They occur in the early phase of joint degeneration when structural abnormalities of the cartilage are not visible on conventional MRA, plain radiography or intraoperatively. Biochemically sensitive MRI sequences for cartilage include the techniques of delayed gadolinium enhanced MRI of cartilage (dGEMRIC; Fig. 9), T2/T2* mapping and T1ρ (T1-rho).

dGEMRIC

Glycosaminoglycans (GAG) are a negatively charged polysaccharides that highly attract water and serve as a lubricant or shock absorber. High contents are found in the extracellular matrix of healthy cartilage. A reduction of GAG is associated with an early, histochemical change in degenerative joint disease [17]. Negatively charged gadolinium-based contrast agents reduce T1 relaxation time ($T1_{Gd}$). They distribute in cartilage in an inverse relationship to the content of GAG [107–110]. Therefore, higher $T1_{Gd}$ values are enriched in healthy cartilage, lower $T1_{Gd}$ diseased cartilage (Fig. 9). Most commonly, the double negatively charged contrast agent is applied intravenously (Gd-DTPA2^{-}), however, single negatively charged contrast agent (Gd-DOTA^{-}) has been used both intravenously as well as intra-articularly [109, 110]. Both techniques (intra-articular versus intravenous contrast application) generate comparable information [111]. However, $T1_{Gd}$ after intra-articular contrast application was shown to be lower compared with intravenous application [110]. After intravenous contrast application, a 'wash in'-time of 15–90 min is necessary to achieve the best possible sensitivity of $T1_{Gd}$. This time frame is shorter after intra-articular contrast application and is influenced by the thickness of the cartilage layers, and the degree of degeneration [112, 113]. Physical exercise such as walking for 10–15 min immediately after intravenous contrast agent application was shown to increase the delivery of the contrast agent into the articular cartilage [114–116]. In contrast, no exercise is recommended after intra-articular

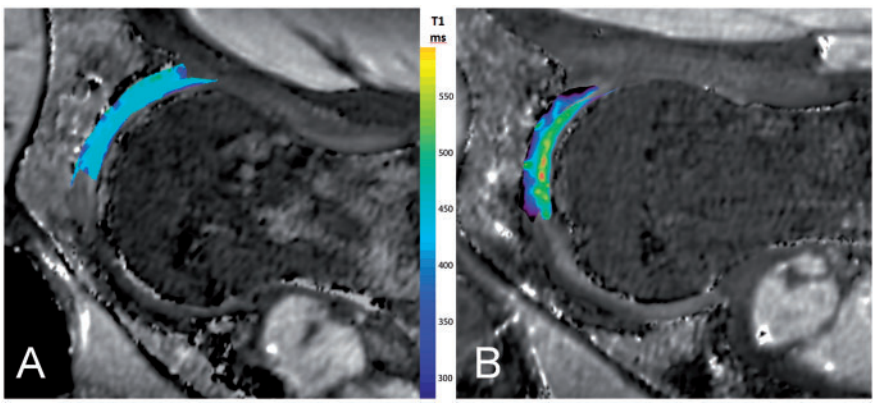

Fig. 9. Anterosuperior radial reformats dGEMRIC scans at 3 Tesla (i.v. contrast injected; 3D dual-flip angle gradient echo-technique) of (A) an asymptomatic woman and (B) a man with symptomatic cam impingement are shown. As T1Gd decreases in an inverse relationship to the amount of glycosaminoglycan content, lower T1Gd values are measured in the diseased acetabular cartilage (dark blue; B).

administration to prevent contrast medium escape from the joint [114]. The need for pre-contrast imaging ($T1_0$) was assessed in several studies. Studies of the knee joint and hip joint assessing the need for pre contrast imaging ($T1_{0)}$ showed high correlation between $T1_{Gd}$ and ΔR (defined as the difference of relaxation rate ($R1 = 1/T1$) between $T1_0$ and $T1_{Gd}$ measurements ($1/T1_{Gd} - 1/T1_0$) [117, 118]. Based on this, it was suggested that isolated $T1_{Gd}$ assessment of the hip joint cartilage is sufficient for the evaluation without the need for expensive and time consuming pre contrast imaging [119]. However, in the setting of cartilage repair therapy (e.g. autologous chondrocyte implantation), pre-contrast imaging for the calculation of ΔR may add to a more accurate GAG evaluation as $T1_0$ values differ from values in normal, hyaline cartilage [120, 121].

2D T1 weighted [122, 123] and 3D $T1_{Gd}$ -sequences [18, 124] are available, the latter allow multiplanar reconstructions for a better geographic evaluation. However, post-processing (e.g. multiplanar reconstruction) is needed for interpretation of the images. Classically the T1 relaxation time is measured manually by defining regions of interest [125, 126] which restricts the routine evolution to just a few selected slices [127]. New automated segmentation methods for assessment of whole-joint dGEMRIC values with presentation as two-dimensional (2D) planar maps have been presented [127, 128]. Several clinical studies have been conducted applying the dGEMRIC technique in hips with FAI. Bittersohl *et al.* found decreased $T1_{Gd}$ values in the anterosuperior region in patients with FAI compared with asymptomatic subjects [129]. Similar damage patterns were reported in another study [130]. Pollard *et al.* found decreased $T1_{Gd}$ values in a population of asymptomatic subjects with a cam deformity compared with morphologically normal hips [131] with an inverse linear correlation between the extent of alpha-angles and the $T1_{Gd}$ [131]. These findings were confirmed in another study [132]. Despite technical developments and promising results in clinical studies as well as standardized protocols, direct clinical implementation of dGEMRIC based on the results obtained from previous studies is not recommended [17, 18, 131], as several factors related to the individual tissue properties or acquisition techniques bear the risk for false interpretations and restrict direct comparability.

T2/T2* mapping

T2 relaxation time is increased with decreased water and collagen fiber integrity, both of which is found in an early stage of cartilage degeneration [133–135]. Subburaj *et al.* reported higher T2 relaxations times in the cartilage of FAI patients compared with asymptomatic volunteers [136]. An ovine study conducted 3 Tesla MRI on Swiss alpine sheep 10–14 weeks after surgically inducing cam-type FAI [137]. Negative correlation between T2 relaxation values and the histological ranking of OA according to Mankin [138, 139] with a positive predictive value of 100% and a negative predicted value of 84% was noted [140].

Similarly to the T2, T2* mapping measures water content in the cartilage as well as the interaction with hydrophilic collagen fibers [141]. However, on a physical level, both techniques differ distinctly. The T2 technique is based on a T2 spin echo sequence comprising a 180°spin rephasing radio frequency pulse. The T2* technique, in contrast, is conducted based on a gradient echo pulse lacking the 180° refocusing pulse. This leads to faster acquisition times of the images using the T2*. Another advantage of T2* versus T2 is the possibility to perform high resolution with three dimensional cartilage assessment. Both, T2 and T2* do not require the application of contrast agents (Fig. 10). Bittersohl *et al.* identified decreased T2* relaxation times in 29 hips with FAI compared with 35 asymptomatic volunteers [142]. Another study found an inverse relationship between T2* relaxation times and the Mankin score, and a positive predictive value (negative predictive value) of 100% (94%) to detect advanced cartilage lesions [140]. Apprich *et al.* compared the T2* values of acetabular cartilage between a group of 22 patients with FAI symptoms and a control group of 27 asymptomatic volunteers. With increasing time of unloading of the joint, the authors noted increased T2* values in the control group, and decreased values in the symptomatic group [143].

T1ρ (T1-rho)

GAG content in hyaline cartilage is depicted by T1ρ mapping technique. Unlike dGEMRIC, T1ρ does not require contrast agent. This allows for direct acquisition of the images without the necessity to await contrast agent uptake into the cartilage. However, T1ρ uses a high radio frequency pulse the bears the risk of tissue heating. In a study by Subburaj *et al.*, the authors reported increased T1ρ relaxation times in nine FAI hips compared with 12 asymptomatic controls [136]. Rakhra *et al.* demonstrated a specific T1ρ relaxation time distribution pattern across the level of the cartilage layer: T1ρ relaxation times in asymptomatic volunteers revealed decreasing values from the superficial to the deep level of the cartilage. In the FAI group, this distribution pattern was depleted [144]. Another recent study investigated T1ρ values in the weight-bearing zone of 19 patients with bilateral cam deformities. All patients had unilateral symptoms. The authors did not reveal any differences between the symptomatic and asymptomatic side, and concluded that regardless of hip pain, a cam deformity predisposes to cartilage degradation increasing the risk for OA [145].

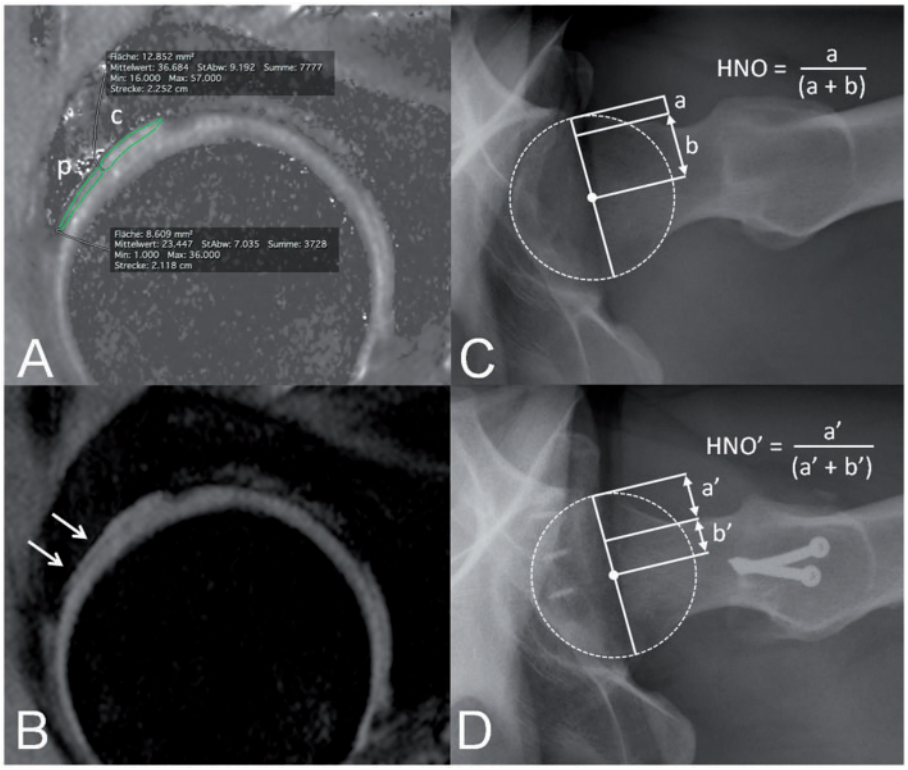

Fig. 10. (A–C) Preoperative imaging of a 35-year-old woman with mixed type FAI. (A) Axial-oblique T2* measurements at 1.5 T (native MRI; two-dimensional gradient echo sequence) show decreased T2* relaxation times in the peripheral compartment (p; T2* = 23 ms) compared with the central department (c; T2* = 36 ms). (B) On the corresponding morphological sequence, no obvious cartilage lesions are depicted apart from cartilage thinning adjacent to the acetabular rim (arrows). (C) Preoperative axial radiographs reveal the cam deformity with decreased femoral head neck offset (HNO). (D) The cam deformity was corrected resulting in increased head neck offset (HNO'). Acetabular rim trimming and labrum refixation was performed to address the pincer component.

COMPUTED TOMOGRAPHY

The role of computed tomography (CT) in the primary diagnostic process of patients suffering FAI is limited. Due to better bone to soft tissue contrast properties with CT, 3D assessment of purely osseous pathologies is superior compared with MRI/MRA (Fig. 11). To dynamically assess FAI, computer-assisted-image-guiding software tools have been developed [19, 146]. These programs are based on CT data of the pelvis and the proximal and distal femur exposing the femoral condyles. Because of its excellent bone to soft tissue contrast properties CT is the method of choice [147]. One software called HipMotion [19, 146] is based on two coordinate systems, one for the femur using the femoral head center, the mechanical axis and the femoral condyles as landmarks and another one for the pelvis using the anterior superior iliac spines and pubic tubercles (anterior pelvic plane) as landmarks [21, 37, 148, 149]. After automated segmentation of the volumetric CT data, algorithms for hip motion patterns are implemented [19, 146]. Virtual range of motion (ROM) simulation allows detection of potential sources of intra- and extra-articular impingement (Fig. 12), and treatment simulation can be conducted by virtually resecting the acetabular rim or performing a head-neck osteochondroplasty [20].

CT based image-guiding software tools are increasingly used for patients suffering FAI. Frequently, complex deformities of the hip such as sequelae of Legg-Calvé-Perthes disease, slipped capital femoral epiphysis, proximal femoral deficiency or torsional alterations of the femur require a more detailed preoperative assessment to better understand the dynamic pathomechanism [21, 66, 150–154]. Computer-assisted image-guiding software tools are also applied in the pre-clinical setting. In a study by Kubiak-Langer *et al.*, the effects of virtual osteochondroplasty in hips with impingement morphologies on the ROM pattern were studied. The authors reported a restoration ROM after virtual correction of the head-neck offset to the degree of normal hips [20]. Another study analyzed ROM patterns in hips with sequelae of LCPD revealing complex motion patterns with both intra- and extra-articular impingement conflicts [152]. Siebenrock *et al.* shed light on the necessity to address torsional deformities of the femur in FAI. Hips with a valgus deformity and high antetorsion had distinctly different

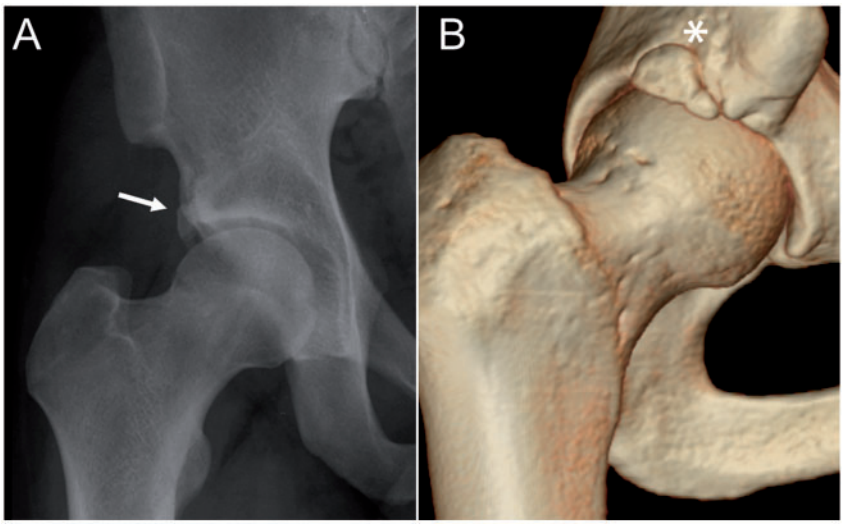

Fig. 11. The preoperative images of a 27 years old patient male patient with right hip pain after an old basketball injury are shown. (A) The AP radiograph reveals an irregularity of the superior acetabular wall (arrow). (B) A three dimensional reconstruction of a CT scan reveals a malunited antero-superior acetabular wall fracture causing focal over-coverage and subsequent pincer type FAI (asterisk). After removal and acetabular rim trimming at the site of the malunion through a surgical hip dislocation, the patient was pain free with unlimited hip function.

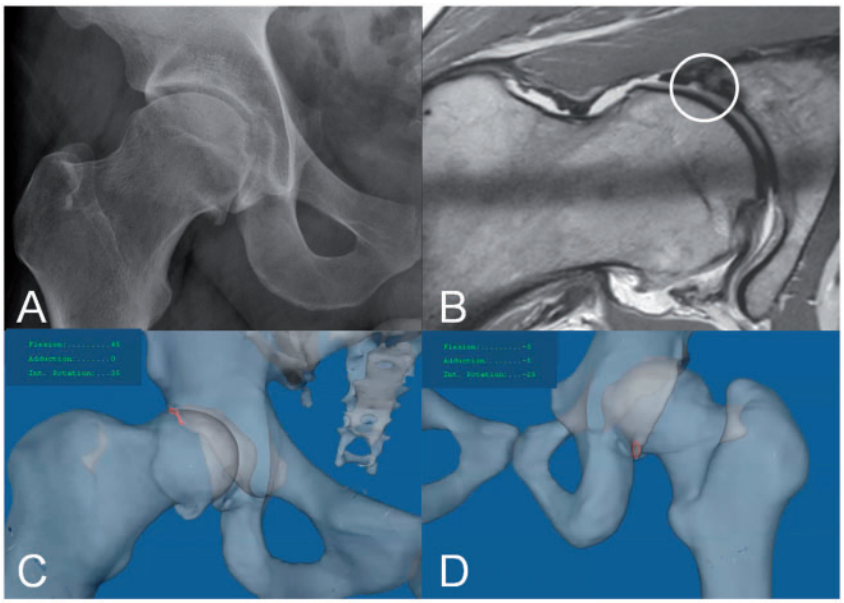

Fig. 12. Complex case of cam impingement in a 30-year-old man. (A) AP pelvic view and (B) radial MRA demonstrate supero-lateral cam and postero-inferior secondary osteophyte. (B) Joint space narrowing at the acetabular rim and adjacent partial labrum tear. (C) CT based dynamic impingement simulation confirms early anterosuperior abutment with flexion and internal rotation (red area) and (D) postero-inferior provoked in extension, abduction and external rotation (red area).

motion patterns compared with normal hips [66]. Despite their practicability, there are drawbacks to these applications. These include radiation exposure during image acquisition (dose range: 6–8 mSv), limited availability and high costs of sophisticated software packages. Although MRI is increasingly used for automated segmentation to avoid radiation [155–157], applications for dynamic assessment of FAI such as virtual ROM simulation based on CT data is superior compared with MRI mainly due to the decreased contrast threshold between bone and soft tissue.

SUMMARY AND FUTURE PERSPECTIVES

As our understanding of the pathologies and mechanisms associated with FAI continue to evolve there is a need for simultaneous advances in both static and dynamic imaging techniques. In particular, there is a need for better evaluation of articular cartilage status to allow both assessments of patients who may benefit from FAI surgery as well as allowing long term evaluation of the results of surgery. The acquisition of plain radiographs and MRA as primary imaging modalities is essential prior to treatment planning. CT based software tools allow dynamic assessment of FAI, however, MRI based techniques to avoid exposure to radiation in the mainly young patient population are desirable. In addition, image guided intraoperative navigation tools for FAI surgery have not been established for routine clinical use. The goal of hip joint preserving surgery is to improve pain and function, and to delay or prevent the onset of osteoarthritis. Recognition of pre-existing degenerative changes at an early stage is crucial to achieve this goal. Biochemical MRI has opened up a new field to noninvasively detect early stage cartilage degeneration. Although preliminary results are promising, it remains an ongoing subject of research and future developments are necessary to allow the wide spread use.

FUNDING

No external funding was received.

ACKNOWLEDGEMENTS

None.

REFERENCES

1. Ganz R, Parvizi J, Beck M *et al*. Femoroacetabular impingement: a cause for osteoarthritis of the hip. *Clin Orthop Relat Res* 2003; **417**: 112–20.
2. Ganz R, Gill TJ, Gautier E *et al*. Surgical dislocation of the adult hip a technique with full access to the femoral head and acetabulum without the risk of avascular necrosis. *J Bone Joint Surg Br Vol* 2001; **83**: 1119–24.
3. Philippon MJ, Stubbs AJ, Schenker ML *et al*. Arthroscopic management of femoroacetabular impingement: osteoplasty technique and literature review. *Am J Sports Med* 2007; **35**: 1571–80.
4. Steppacher SD, Anwander H, Zurmuhle CA *et al*. Eighty percent of patients with surgical hip dislocation for femoroacetabular impingement have a good clinical result without osteoarthritis progression at 10 years. *Clin Orthop Relat Res* 2015; **473**: 1333–41.
5. Beaule PE, Le Duff MJ, Zaragoza E. Quality of life following femoral head-neck osteochondroplasty for femoroacetabular impingement. *J Bone Joint Surg Am* 2007; **89**: 773–9.
6. Beck M, Leunig M, Parvizi J *et al*. Anterior femoroacetabular impingement: part II. *Midterm Results of Surgical Treatment. Clin Orthop Relat Res* 2004; **418**: 67–73.
7. Byrd JW, Jones KS. Arthroscopic management of femoroacetabular impingement: minimum 2-year follow-up. *Arthroscopy* 2011; **27**: 1379–88.
8. Chiron P, Espie A, Reina N *et al*. Surgery for femoroacetabular impingement using a minimally invasive anterolateral approach: analysis of 118 cases at 2.2-year follow-up. *Orthop Traumatol Surg Res* 2012; **98**: 30–8.
9. Jackson TJ, Hanypsiak B, Stake CE *et al*. Arthroscopic labral base repair in the hip: clinical results of a described technique. *Arthroscopy* 2014; **30**: 208–13.
10. Laude F, Sariali E, Nogier A. Femoroacetabular impingement treatment using arthroscopy and anterior approach. *Clin Orthop Relat Res* 2009; **467**: 747–52.
11. Murphy S, Tannast M, Kim YJ *et al*. Debridement of the adult hip for femoroacetabular impingement: indications *and preliminary clinical results. Clin Orthop Relat Res* 2004; **429**: 178–81.
12. Naal FD, Miozzari HH, Wyss TF *et al*. Surgical hip dislocation for the treatment of femoroacetabular impingement in high-level athletes. *Am J Sports Med* 2011; **39**: 544–50.
13. Palmer DH, Ganesh V, Comfort T *et al*. Midterm outcomes in patients with cam femoroacetabular impingement treated arthroscopically. *Arthroscopy* 2012; **28**: 1671–81.
14. Peters CL, Schabel K, Anderson L *et al*. Open treatment of femoroacetabular impingement is associated with clinical improvement and low complication rate at short-term followup. *Clin Orthop Relat Res* 2010; **468**: 504–10.
15. Philippon MJ, Briggs KK, Yen YM *et al*. Outcomes following hip arthroscopy for femoroacetabular impingement with associated chondrolabral dysfunction: minimum two-year follow-up. *J Bone Joint Surg Br* 2009; **91**: 16–23.
16. Tannast M, Siebenrock KA, Anderson SE. Femoroacetabular impingement: radiographic diagnosis-what the radiologist should know. *AJR Am J Roentgenol* 2007; **188**: 1540–52.
17. Bittersohl B, Hosalkar HS, Hesper T *et al*. Advanced imaging in femoroacetabular impingement: current state and future prospects. *Front Surg* 2015; **2**: 34.
18. Lattanzi R, Petchprapa C, Ascani D *et al*. Detection of cartilage damage in femoroacetabular impingement with standardized dGEMRIC at 3 T. *Osteoarthritis Cartilage* 2014; **22**: 447–56.
19. Puls M, Ecker TM, Tannast M *et al*. The Equidistant Method—a novel hip joint simulation algorithm for detection of femoroacetabular impingement. *Comput Aided Surg* 2010; **15**: 75–82.
20. Kubiak-Langer M, Tannast M, Murphy SB *et al*. Range of motion in anterior femoroacetabular impingement. *Clin Orthop Relat Res* 2007; **458**: 117–24.
21. Tannast M, Kubiak-Langer M, Langlotz F *et al*. Noninvasive three-dimensional assessment of femoroacetabular impingement. *J Orthop Res* 2007; **25**: 122–31.
22. Beck M, Kalhor M, Leunig M *et al*. Hip morphology influences the pattern of damage to the acetabular cartilage: femoroacetabular impingement as a cause of early osteoarthritis of the hip. *J Bone Joint Surg Br* 2005; **87**: 1012–8.
23. Siebenrock KA, Schoeniger R, Ganz R. Anterior femoroacetabular impingement due to acetabular retroversion. Treatment with periacetabular osteotomy. *J Bone Joint Surg Am* 2003; **85-A**: 278–86.

24. Albers CE, Steppacher SD, Ganz R *et al*. Joint-preserving surgery improves pain, range of motion, and abductor strength after Legg-Calve-Perthes disease. *Clin Orthop Relat Res* 2012; **470**: 2450–61.
25. Albers CE, Steppacher SD, Haefeli PC *et al*. Twelve Percent of hips with a primary cam deformity exhibit a slip-like morphology resembling sequelae of slipped capital femoral epiphysis. *Clin Orthop Relat Res* 2015; **473**: 1212–23.
26. Wensaas A, Gunderson RB, Svenningsen S *et al*. Femoroacetabular impingement after slipped upper femoral epiphysis: the radiological diagnosis and clinical outcome at long-term follow-up. *J Bone Joint Surg Br* 2012; **94**: 1487–93.
27. Eijer H, Myers SR, Ganz R. Anterior femoroacetabular impingement after femoral neck fractures. *J Orthop Trauma* 2001; **15**: 475–81.
28. Tönnis D. Gerneral radiography of the hip joint. In: Tönnis D (ed). *Congenital Dysplasia, Dislocation of the Hip*. New York, NY: Springer, 1987,100–42.
29. Tannast M, Siebenrock KA. Imaging: Plain Radiographs. In: Sekiya JK, Safran MR, Ranawat AS, Leunig M, (eds). *Techniques in Hip Arthroscopy and Joint Preservation*. Philadelphia: Elsevier Saunders, 2011,23–4.
30. Burckhardt K. *Theoretical study to the sub-project 'interactive software for 2D and 3D standardization of pelvic radiographs and CT-scans for accurate evaluation of hip joint morphology' under CO-ME project 4*. Zürich: Swiss Federal Institute of Technology, 2003, 267.
31. Tannast M, Fritsch S, Zheng G *et al*. Which radiographic hip parameters do not have to be corrected for pelvic rotation and tilt? *Clin Orthop Relat Res* 2015; **473**: 1255–66.
32. Tannast M, Mistry S, Steppacher SD *et al*. Radiographic analysis of femoroacetabular impingement with Hip2Norm-reliable and validated. *J Orthop Res* 2008; **26**: 1199–205.
33. Tannast M, Zheng G, Anderegg C *et al*. Tilt and rotation correction of acetabular version on pelvic radiographs. *Clin Orthop Relat Res* 2005; **438**: 182–90.
34. Steppacher SD, Albers CE, Tannast M *et al*. Plain Radiographic Evaluation of the Hip. In: Nho SH, Leunig M, Larson CM, Bedi A, Kelly BT (eds). *Hip Arthroscopy and Hip Joint Preservation Surgery*. New York/Heidelberg/Dordrecht/London: Springer, 2015, 33–51.
35. Buchler L, Schwab JM, Whitlock PW *et al*. Intraoperative evaluation of acetabular morphology in hip arthroscopy comparing standard radiography versus fluoroscopy: a cadaver study. *Arthroscopy* 2016; **32**: 1030–7.
36. Siebenrock KA, Kalbermatten DF, Ganz R. Effect of pelvic tilt on acetabular retroversion: a study of pelves from cadavers. *Clin Orthop Relat Res* 2003; **407**: 241–8.
37. Tannast M, Langlotz U, Siebenrock KA *et al*. Anatomic referencing of cup orientation in total hip arthroplasty. *Clin Orthop Relat Res* 2005; **436**: 144–50.
38. Drenckhahn D, Eckstein F. *Untere Extremität*. Drenckhahn D (ed.). München: Urban & Fischer, 2003.
39. Lierse W. *Praktische Anatomie*. Lantz T, Wachsmuth W (eds.). Berlin: Springer, 1988.
40. Williams PL. *The skeleton of the lower limb*. Williams PL, Warkick R, Dyson M, Bannister LH (eds.). Edinburgh, UK: Churchill Livingstone: Gray's Anatomy, 1989.
41. Wiberg G. The anatomy and roentgenographic appearance of a normal hip joint. *Acta Chir Scand* 1939; **83**: 7–38.
42. Idelberger K, Frank A. [A new method for determination of the angle of the pevic acetabulum in child and in adult]. *Z Orthop Ihre Grenzgeb* 1952; **82**: 571–7.
43. Sharp IK. Acetabular dysplasia: the acetabular angle. *J Bone Joint Surg Br* 1961; **43**: 268–7.
44. Reynolds D, Lucas J, Klaue K. Retroversion of the acetabulum. A cause of hip pain. *J Bone Joint Surg Br* 1999; **81**: 281–8.
45. Zheng G, Tannast M, Anderegg C *et al*. Hip2Norm: an object-oriented cross-platform program for 3D analysis of hip joint morphology using 2D pelvic radiographs. *Comput Methods Programs Biomed* 2007; **87**: 36–45.
46. Clohisy JC, Carlisle JC, Beaule PE *et al*. A systematic approach to the plain radiographic evaluation of the young adult hip. *J Bone Joint Surg Am* 2008; **90 Suppl 4**: 47–66.
47. Dunn DM. Anteversion of the neck of the femur; a method of measurement. *J Bone Joint Surg Br* 1952; **34-B**: 181–6.
48. Rippstein J. [Determination of the antetorsion of the femur neck by means of two x-ray pictures]. *Z Orthop Ihre Grenzgeb* 1955; **86**: 345–60.
49. Lauenstein C. Nachweis der Ḱocherschen Verbiegunǵdes Schenkelhalses bei der Coxa vara durch Röntgenstrahlen. *Fortschr Röntgenstr* 1901; **4**: 61–4.
50. Lequesne M, de S. False profile of the pelvis. A new radiographic incidence for the study of the hip. Its use in dysplasias and different coxopathies. *Rev Rhum Mal Osteoartic* 1961; **28**: 643–52.
51. Nepple JJ, Brophy RH, Matava MJ *et al*. Radiographic findings of femoroacetabular impingement in National Football League Combine athletes undergoing radiographs for previous hip or groin pain. *Arthroscopy* 2012; **28**: 1396–403.
52. Tonnis D, Heinecke A. Acetabular and femoral anteversion: relationship with osteoarthritis of the hip. *J Bone Joint Surg Am* 1999; **81**: 1747–70.
53. Murphy SB, Ganz R, Muller ME. The prognosis in untreated dysplasia of the hip. A study of radiographic factors that predict the outcome. *J Bone Joint Surg Am* 1995; **77**: 985–9.
54. Tannast M, Hanke MS, Zheng G *et al*. What are the radiographic reference values for acetabular under- and overcoverage?. *Clin Orthop Relat Res* 2015; **473**: 1234–46.
55. Ecker TM, Tannast M, Puls M *et al*. Pathomorphologic alterations predict presence or absence of hip osteoarthrosis. *Clin Orthop Relat Res* 2007; **465**: 46–52.
56. Clohisy JC, Dobson MA, Robison JF *et al*. Radiographic structural abnormalities associated with premature, natural hip-joint failure. *J Bone Joint Surg Am* 2011; **93 Suppl 2**: 3–9.
57. Siebenrock KA, Kistler L, Schwab JM *et al*. The acetabular wall index for assessing anteroposterior femoral head coverage in symptomatic patients. *Clin Orthop Relat Res* 2012; **470**: 3355–60.
58. Kalberer F, Sierra RJ, Madan SS *et al*. Ischial spine projection into the pelvis: a new sign for acetabular retroversion. *Clin Orthop Relat Res* 2008; **466**: 677–83.
59. Tannast M, Pfannebecker P, Schwab JM *et al*. Pelvic morphology differs in rotation and obliquity between developmental dysplasia of the hip and retroversion. *Clin Orthop Relat Res* 2012; **470**: 3297–305.

60. Steppacher SD, Lerch TD, Gharanizadeh K *et al*. Size and shape of the lunate surface in different types of pincer impingement: theoretical implications for surgical therapy. *Osteoarthritis Cartilage* 2014; **22**: 951–8.
61. Notzli HP, Wyss TF, Stoecklin CH *et al*. The contour of the femoral head-neck junction as a predictor for the rick of anterior impingement. *J Bone Joint Surg Br* 2002; **84**: 556–60.
62. Toogood PA, Skalak A, Cooperman DR. Proximal femoral anatomy in the normal human population. *Clin Orthop Relat Res* 2009; **467**: 876–85.
63. Ito K, Minka MA, 2nd *et al*. Femoroacetabular impingement and the cam-effect. A MRI-based quantitative anatomical study of the femoral head-neck offset. *J Bone Joint Surg Br* 2001; **83**: 171–6.
64. Stulberg SD, Cordell LD, Harris WH *et al*. Unrecognized childhood hip disease: a major cause of idiopathic osteoarthritis of the hip. In: The Hip. Proceedings of the 3rd meeting of The Hip Society. St Louis: CV Mosby Co., 1975, 121–28.
65. Apley AG, Wientroub S. The sagging rope sign in Perthes' disease and allied disorders. *J Bone Joint Surg Br* 1981; **63**: 43–7.
66. Siebenrock KA, Steppacher SD, Haefeli PC *et al*. Valgus hip with high antetorsion causes pain through posterior extraarticular FAI. *Clin Orthop Relat Res* 2013; **471**: 3774–80.
67. Hoaglund FT, Low WD. Anatomy of the femoral neck and head, with comparative data from Caucasians and Hong Kong Chinese. *Clin Orthop Relat Res* 1980; **152**: 10–6.
68. Müller ME. *Die hüftnahen Femurosteotomien unter Berücksichtigung der Form, Funktion und Beanspruchung des Hüftgelenkes*. Stuttgart: Thieme, 1957.
69. Hack K, Di Primio G, Rakhra K *et al*. Prevalence of cam-type femoroacetabular impingement morphology in asymptomatic volunteers. *J Bone Joint Surg Am* 2010; **92**: 2436–44.
70. Jung KA, Restrepo C, Hellman M *et al*. The prevalence of cam-type femoroacetabular deformity in asymptomatic adults. *J Bone Joint Surg Br* 2011; **93**: 1303–7.
71. Laborie LB, Lehmann TG, Engesaeter IO *et al*. Prevalence of radiographic findings thought to be associated with femoroacetabular impingement in a population-based cohort of 2081 healthy young adults. *Radiology* 2011; **260**: 494–502.
72. Rubin DA. Femoroacetabular impingement: fact, fiction, or fantasy? *AJR Am J Roentgenol* 2013; **201**: 526–34.
73. Ochoa LM, Dawson L, Patzkowski JC *et al*. Radiographic prevalence of femoroacetabular impingement in a young population with hip complaints is high. *Clin Orthop Relat Res* 2010; **468**: 2710–4.
74. Chakraverty JK, Sullivan C, Gan C *et al*. Cam and pincer femoroacetabular impingement: CT findings of features resembling femoroacetabular impingement in a young population without symptoms. *AJR Am J Roentgenol* 2013; **200**: 389–95.
75. Hong RJ, Hughes TH, Gentili A *et al*. Magnetic resonance imaging of the hip. *J Magn Reson Imaging* 2008; **27**: 435–45.
76. Kassarjian A, Cerezal L, Llopis E. MR arthrography of the hip with emphasis on femoroacetabular impingement. *Radiologia* 2009; **51**: 17–29.
77. Klenke FM, Hoffmann DB, Cross BJ *et al*. Validation of a standardized mapping system of the hip joint for radial MRA sequencing. *Skeletal Radiol* 2015; **44**: 339–43.
78. Mamisch TC, Bittersohl B, Hughes T *et al*. Magnetic resonance imaging of the hip at 3 Tesla: clinical value in femoroacetabular impingement of the hip and current concepts. *Semin Musculoskelet Radiol* 2008; **12**: 212–22.
79. Peeters J, Vanhoenacker FM, Marchal P *et al*. Imaging of femoroacetabular impingement: pictorial review. *JBR-BTR* 2009; **92**: 35–42.
80. Pfirrmann CW, Duc SR, Zanetti M *et al*. MR arthrography of acetabular cartilage delamination in femoroacetabular cam impingement. *Radiology* 2008; **249**: 236–41.
81. Pfirrmann CW, Mengiardi B, Dora C *et al*. Cam and pincer femoroacetabular impingement: characteristic MR arthrographic findings in 50 patients. *Radiology* 2006; **240**: 778–85.
82. Albers CE, Schwarz A, Hanke MS *et al*. Acetabular version increases after closure of the triradiate cartilage complex. *Clin Orthop Relat Res* 2016; epub ahead of print.
83. Dudda M, Albers C, Mamisch TC *et al*. Do normal radiographs exclude asphericity of the femoral head-neck junction? *Clin Orthop Relat Res* 2009; **467**: 651–9.
84. Saito M, Tsukada S, Yoshida K *et al*. Correlation of alpha angle between various radiographic projections and radial magnetic resonance imaging for cam deformity in femoral head-neck junction. *Knee Surg Sports Traumatol Arthrosc* 2016; epub ahead of print.
85. Hingsammer AM, Bixby S, Zurakowski D *et al*. How do acetabular version and femoral head coverage change with skeletal maturity?. *Clin Orthop Relat Res* 2015; **473**: 1224–33.
86. Dandachli W, Ul Islam S, Tippett R *et al*. Analysis of acetabular version in the native hip: comparison between 2D axial CT and 3D CT measurements. *Skeletal Radiol* 2011; **40**: 877–83.
87. Monazzam S, Bomar JD, Dwek JR *et al*. Development and prevalence of femoroacetabular impingement-associated morphology in a paediatric and adolescent population: a CT study of 225 patients. *Bone Joint J* 2013; **95-B**: 598–604.
88. Anderson LA, Peters CL, Park BB *et al*. Acetabular cartilage delamination in femoroacetabular impingement. Risk factors and magnetic resonance imaging diagnosis. *J Bone Joint Surg Am* 2009; **91**: 305–13.
89. Clohisy JC, St John LC, Schutz AL. Surgical treatment of femoroacetabular impingement: a systematic review of the literature. *Clin Orthop Relat Res* 2010; **468**: 555–64.
90. Schmaranzer F, Klauser A, Kogler M *et al*. Diagnostic performance of direct traction MR arthrography of the hip: detection of chondral and labral lesions with arthroscopic comparison. *Eur Radiol* 2015; **25**: 1721–30.
91. Safran MR, Hariri S. Hip arthroscopy assessment tools and outcomes. *Oper Tech Orthop* 2010; **20**: 264–77.
92. Griffin D, Karthikeyan S. Normal and pathological arthroscopic view in hip arthroscopy. In: Marín-Peña Ó (ed.). *Femoroacetabular Impingement*. Berlin, Heidelberg: Springer, 2012, 113–22.
93. Czerny C, Hofmann S, Urban M *et al*. MR arthrography of the adult acetabular capsular-labral complex: correlation with surgery and anatomy. *AJR Am J Roentgenol* 1999; **173**: 345–9.
94. Sutter R, Zubler V, Hoffmann A *et al*. Hip MRI: how useful is intraarticular contrast material for evaluating surgically proven lesions of the labrum and articular cartilage? *Am J Roentgenol* 2014; **202**: 160–9.
95. Smith TO, Hilton G, Toms AP *et al*. The diagnostic accuracy of acetabular labral tears using magnetic resonance imaging and magnetic resonance arthrography: a meta-analysis. *Eur Radiol* 2011; **21**: 863–74.

96. Toomayan GA, Holman WR, Major NM *et al*. Sensitivity of MR arthrography in the evaluation of acetabular labral tears. *Am J Roentgenol* 2006; **186**: 449–53.
97. Magee T. Comparison of 3.0-T MR vs 3.0-T MR arthrography of the hip for detection of acetabular labral tears and chondral defects in the same patient population. *Br J Radiol* 2015; **88**: 20140817.
98. Yen YM, Kocher MS. Clinical and radiographic diagnosis of femoroacetabular impingement. *J Pediatr Orthop* 2013; **33 Suppl 1**: S112–20.
99. Zlatkin MB, Pevsner D, Sanders TG *et al*. Acetabular labral tears and cartilage lesions of the hip: indirect MR arthrographic correlation with arthroscopy—a preliminary study. *Am J Roentgenol* 2010; **194**: 709–14.
100. Sutter R, Zanetti M, Pfirrmann CW. New developments in hip imaging. *Radiology* 2012; **264**: 651–67.
101. Llopis E, Cerezal L, Kassarjian A *et al*. Direct MR arthrography of the hip with leg traction: feasibility for assessing articular cartilage. *Am J Roentgenol* 2008; **190**: 1124–8.
102. Schmaranzer F, Klauser A, Kogler M *et al*. Improving visualization of the central compartment of the hip with direct MR arthrography under axial leg traction: a feasibility study. *Acad Radiol* 2014; **21**: 1240–7.
103. Suter A, Dietrich TJ, Maier M *et al*. MR findings associated with positive distraction of the hip joint achieved by axial traction. *Skeletal Radiol* 2015; **44**: 787–95.
104. Neumann G, Mendicuti AD, Zou KH *et al*. Prevalence of labral tears and cartilage loss in patients with mechanical symptoms of the hip: evaluation using MR arthrography. *Osteoarthritis Cartilage* 2007; **15**: 909–17.
105. Schmid MR, Notzli HP, Zanetti M *et al*. Cartilage lesions in the hip: diagnostic effectiveness of MR arthrography. *Radiology* 2003; **226**: 382–6.
106. Nepple JJ, Byrd JW, Siebenrock KA *et al*. Overview of treatment options, clinical results, and controversies in the management of femoroacetabular impingement. *J Am Acad Orthop Surg* 2013; **21 Suppl 1**: S53–8.
107. Burstein D, Gray M, Mosher T *et al*. Measures of molecular composition and structure in osteoarthritis. *Radiol Clin North Am* 2009; **47**: 675–86.
108. Williams A, Gillis A, McKenzie C *et al*. Glycosaminoglycan distribution in cartilage as determined by delayed gadolinium-enhanced MRI of cartilage (dGEMRIC): potential clinical applications. *AJR Am J Roentgenol* 2004; **182**: 167–72.
109. Zilkens C, Miese F, Kim YJ *et al*. Three-dimensional delayed gadolinium-enhanced magnetic resonance imaging of hip joint cartilage at 3T: a prospective controlled study. *Eur J Radiol* 2012; **81**: 3420–5.
110. Zilkens C, Miese F, Kim YJ *et al*. Direct comparison of intra-articular versus intravenous delayed gadolinium-enhanced MRI of hip joint cartilage. *J Magn Reson Imaging* 2014; **39**: 94–102.
111. Bittersohl B, Hosalkar HS, Werlen S *et al*. Intravenous versus intra-articular delayed gadolinium-enhanced magnetic resonance imaging in the hip joint—*a comparative analysis. Invest Radiol* 2010; **45**: 538–42.
112. Burstein D, Velyvis J, Scott KT *et al*. Protocol issues for delayed Gd(DTPA)(2-)-enhanced MRI (dGEMRIC) for clinical evaluation of articular cartilage. *Magn Reson Med* 2001; **45**: 36–41.
113. Bittersohl B, Hosalkar HS, Kim YJ *et al*. T1 assessment of hip joint cartilage following intra-articular gadolinium injection: a pilot study. *Magn Reson Med* 2010; **64**: 1200–7.
114. Zilkens C, Tiderius CJ, Krauspe R *et al*. Current knowledge and importance of dGEMRIC techniques in diagnosis of hip joint diseases. *Skeletal Radiol* 2015; **44**: 1073–83.
115. Winalski CS, Aliabadi P, Wright RJ *et al*. Enhancement of joint fluid with intravenously administered gadopentetate dimeglumine: technique, rationale, and implications. *Radiology* 1993; **187**: 179–85.
116. Drape JL, Thelen P, Gay-Depassier P *et al*. Intraarticular diffusion of Gd-DOTA after intravenous injection in the knee: MR imaging evaluation. *Radiology* 1993; **188**: 227–34.
117. Williams A, Mikulis B, Krishnan N *et al*. Suitability of T(1Gd) as the dGEMRIC index at 1.5T and 3.0T. *Magn Reson Med* 2007; **58**: 830–4.
118. Bittersohl B, Hosalkar HS, Kim YJ *et al*. Delayed gadolinium-enhanced magnetic resonance imaging (dGEMRIC) of hip joint cartilage in femoroacetabular impingement (FAI): are pre- and postcontrast imaging both necessary? *Magn Reson Med* 2009; **62**: 1362–7.
119. Bittersohl B, Zilkens C, Kim YJ *et al*. Delayed gadolinium-enhanced magnetic resonance imaging of hip joint cartilage: pearls and pitfalls. *Orthop Rev (Pavia)* 2011; **3**: e11.
120. Watanabe A, Wada Y, Obata T *et al*. Delayed gadolinium-enhanced MR to determine glycosaminoglycan concentration in reparative cartilage after autologous chondrocyte implantation: preliminary results. *Radiology* 2006; **239**: 201–8.
121. Trattnig S, Mamisch TC, Pinker K *et al*. Differentiating normal hyaline cartilage from post-surgical repair tissue using fast gradient echo imaging in delayed gadolinium-enhanced MRI (dGEMRIC) at 3 Tesla. *Eur Radiol* 2008; **18**: 1251–9.
122. Tiderius CJ, Olsson LE, Leander P *et al*. Delayed gadolinium-enhanced MRI of cartilage (dGEMRIC) in early knee osteoarthritis. *Magn Reson Med* 2003; **49**: 488–92.
123. Bashir A, Gray ML, Hartke J *et al*. Nondestructive imaging of human cartilage glycosaminoglycan concentration by MRI. *Magn Reson Med* 1999; **41**: 857–65.
124. Bittersohl B, Hosalkar HS, Haamberg T *et al*. Reproducibility of dGEMRIC in assessment of hip joint cartilage: a prospective study. *J Magn Reson Imaging* 2009; **30**: 224–8.
125. Bittersohl B, Hosalkar HS, Werlen S *et al*. dGEMRIC and subsequent T1 mapping of the hip at 1.5 Tesla: normative data on zonal and radial distribution in asymptomatic volunteers. *J Magn Reson Imaging* 2011; **34**: 101–6.
126. Domayer SE, Mamisch TC, Kress I *et al*. Radial dGEMRIC in developmental dysplasia of the hip and in femoroacetabular impingement: preliminary results. *Osteoarthritis Cartilage* 2010; **18**: 1421–8.
127. Siversson C, Akhondi-Asl A, Bixby S *et al*. Three-dimensional hip cartilage quality assessment of morphology and dGEMRIC by planar maps and automated segmentation. *Osteoarthritis Cartilage* 2014; **22**: 1511–5.
128. Bulat E, Bixby SD, Siversson C *et al*. Planar dGEMRIC maps may aid imaging assessment of cartilage damage in femoroacetabular impingement. *Clin Orthop Relat Res* 2016; **474**: 467–78.
129. Bittersohl B, Steppacher S, Haamberg T *et al*. Cartilage damage in femoroacetabular impingement (FAI): preliminary results on

comparison of standard diagnostic vs delayed gadolinium-enhanced magnetic resonance imaging of cartilage (dGEMRIC). *Osteoarthritis Cartilage* 2009; **17**: 1297–306.
130. Mamisch TC, Kain MS, Bittersohl B *et al*. Delayed gadolinium-enhanced magnetic resonance imaging of cartilage (dGEMRIC) in Femoacetabular impingement. *J Orthop Res* 2011; **29**: 1305–11.
131. Pollard TC, McNally EG, Wilson DC *et al*. Localized cartilage assessment with three-dimensional dGEMRIC in asymptomatic hips with normal morphology and cam deformity. *J Bone Joint Surg Am* 2010; **92**: 2557–69.
132. Jessel RH, Zilkens C, Tiderius C *et al*. Assessment of osteoarthritis in hips with femoroacetabular impingement using delayed gadolinium enhanced MRI of cartilage. *J Magn Reson Imaging* 2009; **30**: 1110–5.
133. Mosher TJ, Dardzinski BJ. Cartilage MRI T2 relaxation time mapping: overview and applications. *Semin Musculoskelet Radiol* 2004; **8**: 355–68.
134. Nieminen MT, Rieppo J, Toyras J *et al*. T2 relaxation reveals spatial collagen architecture in articular cartilage: a comparative quantitative MRI and polarized light microscopic study. *Magn Reson Med* 2001; **46**: 487–93.
135. Liess C, Lusse S, Karger N *et al*. Detection of changes in cartilage water content using MRI T2-mapping in vivo. *Osteoarthritis Cartilage* 2002; **10**: 907–13.
136. Subburaj K, Valentinitsch A, Dillon AB *et al*. Regional variations in MR relaxation of hip joint cartilage in subjects with and without femoralacetabular impingement. *Magn Reson Imaging* 2013; **31**: 1129–36.
137. Siebenrock KA, Fiechter R, Tannast M *et al*. Experimentally induced cam impingement in the sheep hip. *J Orthop Res* 2013; **31**: 580–7.
138. Mankin HJ. The reaction of articular cartilage to injury and osteoarthritis (second of two parts). *N Engl J Med* 1974; **291**: 1335–40.
139. Mankin HJ. The reaction of articular cartilage to injury and osteoarthritis (first of two parts). *N Engl J Med* 1974; **291**: 1285–92.
140. Siebenrock KA, Kienle KP, Steppacher SD *et al*. Biochemical MRI predicts hip osteoarthritis in an experimental ovine femoroacetabular impingement model. *Clin Orthop Relat Res* 2015; **473**: 1318–24.
141. Keenan KE, Besier TF, Pauly JM *et al*. Prediction of glycosaminoglycan content in human cartilage by age, T1rho and T2 MRI. *Osteoarthritis Cartilage* 2011; **19**: 171–9.
142. Bittersohl B, Miese FR, Hosalkar HS *et al*. T2* mapping of acetabular and femoral hip joint cartilage at 3 T. *a prospective controlled study. Invest Radiol* 2012; **47**: 392–7.
143. Apprich S, Mamisch TC, Welsch GH *et al*. Evaluation of articular cartilage in patients with femoroacetabular impingement (FAI) using T2* mapping at different time points at 3.0 Tesla MRI: a feasibility study. *Skeletal Radiol* 2012; **41**: 987–95.
144. Rakhra KS, Lattanzio PJ, Cardenas-Blanco A *et al*. Can T1-rho MRI detect acetabular cartilage degeneration in femoroacetabular impingement?: a pilot study. *J Bone Joint Surg Br* 2012; **94**: 1187–92.
145. McGuffin WS, Melkus G, Rakhra KS *et al*. Is the contralateral hip at risk in patients with unilateral symptomatic cam femoroacetabular impingement? A quantitative T1rho MRI study. *Osteoarthritis Cartilage* 2015; **23**: 1337–42.
146. Puls M, Ecker TM, Steppacher SD *et al*. Automated detection of the osseous acetabular rim using three-dimensional models of the pelvis. *Comput Biol Med* 2011; **41**: 285–91.
147. Ecker TM, Tannast M, Murphy SB. Computed tomography-based surgical navigation for hip arthroplasty. *Clin Orthop Relat Res* 2007; **465**: 100–5.
148. DiGioia AM, Jaramaz B, Blackwell M *et al*. The Otto Aufranc Award. Image guided navigation system to measure intraoperatively acetabular implant alignment. *Clin Orthop Relat Res* 1998; **355**: 8–22.
149. Murphy SB, Simon SR, Kijewski PK *et al*. Femoral anteversion. *J Bone Joint Surg Am* 1987; **69**: 1169–76.
150. Siebenrock KA, Anwander H, Zurmuhle CA *et al*. Head reduction osteotomy with additional containment surgery improves sphericity and containment and reduces pain in Legg-Calve-Perthes disease. *Clin Orthop Relat Res* 2015; **473**: 1274–83.
151. Tannast M, Macintyre N, Steppacher SD *et al*. A systematic approach to analyse the sequelae of LCPD. *Hip Int* 2013; **23 Suppl 9**: S61–70.
152. Tannast M, Hanke M, Ecker TM *et al*. LCPD: reduced range of motion resulting from extra- and intraarticular impingement. *Clin Orthop Relat Res* 2012; **470**: 2431–40.
153. Albers CE, Steppacher SD, Schwab JM *et al*. Relative femoral neck lengthening improves pain and hip function in proximal femoral deformities with a high-riding trochanter. *Clin Orthop Relat Res* 2015; **473**: 1378–87.
154. Ganz R, Huff TW, Leunig M. Extended retinacular soft-tissue flap for intra-articular hip surgery: surgical technique, indications, and results of application. *Instr Course Lect* 2009; **58**: 241–55.
155. Radetzki F, Saul B, Hagel A *et al*. Three-dimensional virtual simulation and evaluation of the femoroacetabular impingement based on black bone MRA. *Arch Orthop Trauma Surg* 2015; **135**: 667–71.
156. Xia Y, Fripp J, Chandra SS *et al*. Automated 3D quantitative assessment and measurement of alpha angles from the femoral head-neck junction using MR imaging. *Phys Med Biol* 2015; **60**: 7601–16.
157. Xia Y, Fripp J, Chandra SS *et al*. Automated bone segmentation from large field of view 3D MR images of the hip joint. *Phys Med Biol* 2013; **58**: 7375–90.